BIBECHANA
A Multidisciplinary Journal of Science, Technology and Mathematics
ISSN 2091-0762 (online)
Journal homepage: http://nepjol.info/index.php/BIBECHANA

Structure, MESP and HOMO-LUMO study of 10-Acetyl-10H-phenothiazine 5-oxide using vibrational spectroscopy and quantum chemical methods

Bhawani Datt Joshi[1,2*], Poonam Tandon[1], Sudha Jain[3]

[1]Department of Physics, University of Lucknow, Lucknow-226007, UP, India
[2]Department of Physics, Siddhanath Sc. Campus, Mahendranagar, Tribhuvan University, Nepal
[3]Department of Chemistry, University of Lucknow, Lucknow-226007, UP, India
[*]Corresponding author: E-mail: bdjoshi_007@yahoo.com
Article history: Received 5 October, 2012; Accepted 7 November, 2012

Abstract

In this communication, we have presented the geometry optimization, complete vibrational study with potential energy distribution (PED) and frontier orbital energy gap for the 10-Acetyl-10H-phenothiazine 5-oxide (APTZ) molecule using *ab initio* Hartree-Fock (HF) and density functional theory (DFT/B3LYP) method employing 6-311++G(d,p) basis set. The calculated IR and Raman spectra with their intensities, molecular electrostatic potential (MESP) surface and highest occupied molecular orbital (HOMO) - lowest unoccupied molecular orbital (LUMO) plot have been given.

Keywords: APTZ; *ab initio*; DFT; IR; Raman; MESP; HOMO - LUMO.

1. Introduction

Phenothiazines, the heterocyclic organic compounds in which sulphur and nitrogen are incorporated in the tricyclic system, exhibit a wide range of pharmacological / biological activities [1-10]. Their several derivatives have been found to possess clinical activities, such as: tranquilizers, antihistamines, diuretics, analgesics, neurolepitcs, anticancer activity [5,6] in vitro (cancer cell lines), antileukemic [5] antimutagenic [2], anti- trypanosomal, antileishmanial [3], and inhibition of the growth of autoimmune deficiency syndrome (AIDS)-related lymphoma cells [4]. Properties of 10-H-phenothiazine, such as: semiconductivity [11], electrical conductivities [12] and low thermal activation energies of charge transfer complexes [13], has opened new practical fields of investigation. Alconea Palafox *et al*. [14] had given a complete vibrational analysis of the Fourier transform (FT) infrared (IR) and FT-Raman spectra of both phenothiazine (PTZ) and N-methylphenothiazine molecules using *ab initio* method as well as quantum chemical calculations. Sharma *et al*. [15] found the better biological activity of 4-thiazolidinone derivatives of phenothiazine. Dixit *et al*. [2] had synthesized some 10H-phenothiazine sulphone derivatives and characterized them with selected bands of IR and 1H NMR spectroscopic methods.

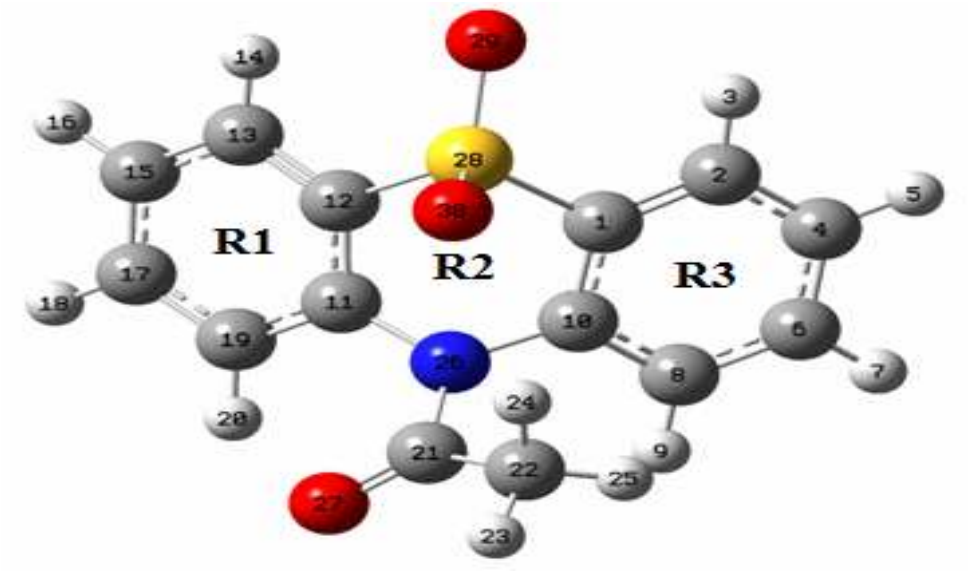

Fig. 1: Optimized structure of APTZ molecule.

Literature survey reveals that neither the vibrational assignments nor the highest molecular orbital (HOMO) - lowest unoccupied molecular orbital (LUMO) study of APTZ derivative of phenothiazine has been studied so far. Thus, a complete vibrational study along with molecular electrostatic potential (MESP) surface and HOMO - LUMO analysis has been carried in the present study using *ab initio* Hartree-Fock (HF) and density functional theory (DFT) method. The vibrational spectroscopy, that deals the short range structure studies, has very keen applications in these days for the structure characterization of biologically active materials [16]. HOMO - LUMO analysis has been performed which helps elucidate charge transfer occurring in the molecule.

2. Methodology
Computational

Geometry optimization, an important issue in molecular mechanics, was performed as the first task of the computational work for the APTZ molecule taking the parameters from the X-ray diffraction data [17]. The optimized ground state molecular structure is shown in Fig. 1. The molecular structure, vibrational frequencies and energy of the optimized geometry of APTZ were computed employing the DFT [18] and HF methods using Gaussian 09 [19] program package employing 6-311++G(d,p) basis set based on Becke's three parameters (local, non-local and Hartree-Fock) hybrid exchange functional with Lee-Yang-Parr correlation functional (B3LYP) [20,21]. The basis set 6-311++G(d,p) augmented by 'd' polarization functions on heavy atoms and 'p' polarization functions on hydrogen atoms as well as diffuse functions for both hydrogen and heavy atoms were used [22,23]. The absolute Raman intensities and IR absorption intensities were calculated in the harmonic approximation at the same level of theory as used for the optimized geometries associated with each normal mode, respectively. The normal mode analysis was performed and the PED was calculated along the internal coordinates using localized symmetry. For this purpose, a complete set of 84 internal coordinates were defined using Pulay's recommendations [24,25]. The vibrational assignments of the normal modes were made on the basis of the PED calculated by using the program GAR2PED [26]. Raman and IR spectra were simulated using a pure Lorentzian band profile (fwhm = 8 cm^{-1}) using indigenously developed software. Visualization and confirmation of calculated data were done by using the CHEMCRAFT program [27].

3. Results and Discussion

3.1. Geometry optimization

Initial geometry taken from X-ray diffraction data [17] of APTZ was minimized without any constraint to the potential energy surface and the optimized structural parameters were used in the vibrational frequency calculation to characterize all stationary points as minima. The molecular conformation from the crystalline structure, as well as yielded by geometry optimization, exhibits no special symmetries. Hence, APTZ molecule crystallizes in the monoclinic, P21/n form having lattice parameters a = 8.1244 (1) Å, b = 14.1787 (2) Å, c = 10.7576 (1) Å, β = 100.963 (1)^{o} and z = 4 in a unit cell [17]. The sulphoxide

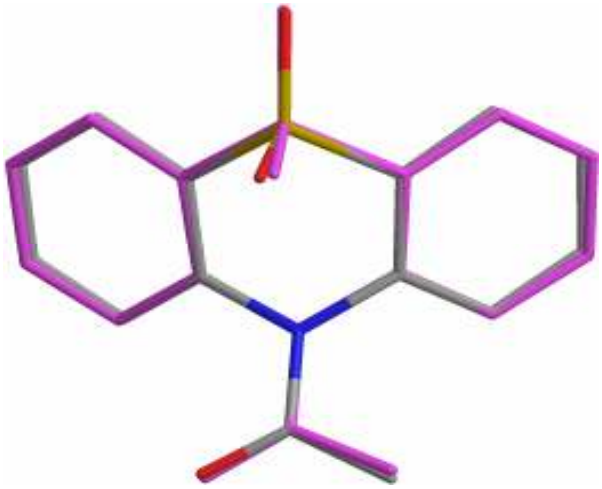

Fig. 2: Comparison of the experimental (from single crystal X-ray diffraction) and optimized structure (purple) of APTZ (hydrogen atoms are excluded for clarity).

oxygen atom is disordered over two sites with occupancies of 0.886 (4) and 0.114 (4), reflecting a partial inversion of the lone pair at the tetrahedral S-atom site. The optimized structure produced is very similar to the experimental one. Both the optimized and experimental structures of the title molecule were compared by superimposing them using a least-squares algorithm that minimizes the distances between the corresponding non-hydrogen atoms as shown in Fig. 2.

3.2. Molecular electrostatic potential surface

In this study, the electrostatic potential (ESP), electron density (ED) and molecular electrostatic potential (MESP) maps for APTZ are as shown in Fig. 3. In ESP, the negative potential is localized near the oxygen atoms and reflects by the yellowish blobs, while the positive potential is localized on the rest surface. However, the ED plot of the title molecule shows uniform distribution. The molecular electrostatic potential (MESP), the force acting on a positive test charge located at point through the electrical charge cloud generated through the net charge of molecule (electrons and nuclei), has been a widely used entity in the chemical literature, generally employed as a tool for probing electron rich regions [28-31]. The MESP at a point 'r' in a molecular framework with nuclear charges Z_A located at R_A and electron density ρ(r) is given by a relation:

$$V(r) = \sum_{A=1}^{N} \frac{Z_A}{|r - R_A|} - \int \frac{\rho(r')}{|r - r'|} d^3r'$$

where N is the total number of nuclei in the molecule. The first term on the right hand side of the above equation represent the contribution due to nucleus and second due to electrons, respectively. When the latter contribution overrides the former one, the net MESP attains a negative value, providing information about electron-rich sites.

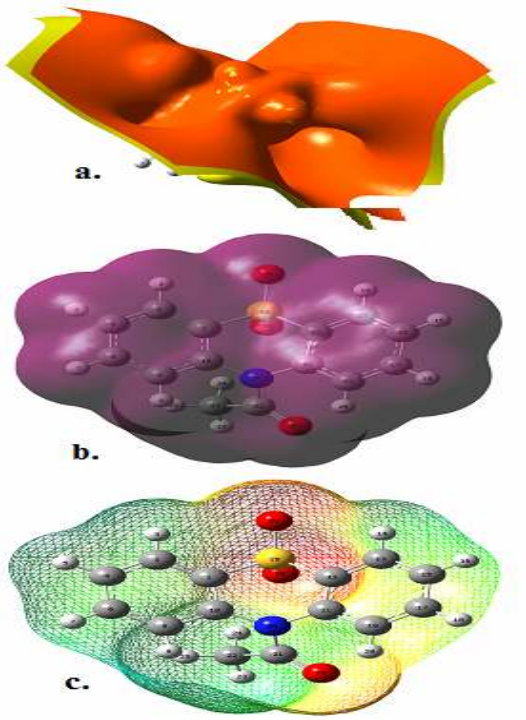

Fig. 3: (a) ESP (b) electron density (c) molecular electrostatic potential mapped on the isodensity surface in the range -6.521x10-2 (red) to +6.521x10-2 (blue) for APTZ.

MESP correlates the total charge distribution with dipole moment, electronegativity, and partial charges and site of chemical reactivity of a molecule. The projection of molecular MESP of APTZ along the molecular plane is given in Fig. 3c. It provides a visual method to understand the relative polarity of a molecule and serves as a useful quantity to explain hydrogen bonding, reactivity and structure-activity relationship of molecules including biomolecules and drugs. It is the potential energy of a proton at a particular location near a molecule. Different values of the electrostatic potential at the surface of a molecule appear with the different colours. In general the attractive (or negative) potential appears in red coloured regions and those of repulsive (or positive) potential appear in blue. In the title molecule the regions near oxygen atoms are most attractive and the regions near hydrogen of methyl group are positive.

3.3. HOMO-LUMO analysis

The HOMO is the outermost (highest energy) orbital containing electrons that could act as an electron donor. The LUMO is the innermost (lowest energy) orbital that has room to accept electrons and can act as the electron acceptor. According to the frontier molecular orbital theory, the formation of a transition state is due to an interaction between the frontier orbitals (HOMO and LUMO) of reactants [32]. The energy of the HOMO is directly related to the ionization potential and the energy of the LUMO is directly related to the electron affinity. High value of HOMO energy is likely to indicate a tendency of the molecule to donate electrons to appropriate acceptor molecule of low empty molecular orbital energy. The lower values of LUMO energy show more probability to accept electrons. So, the gap energy, i.e. the

difference in energy between the HOMO and LUMO, is an important stability index. It is a critical parameter in determining molecular electrical transport properties because it is a measure of electron conductivity. Low gap value refers to the higher electronic transition and vice versa. The HOMO - LUMO plot with the frontier orbital energy gap for the title molecule is shown in Fig. 4.

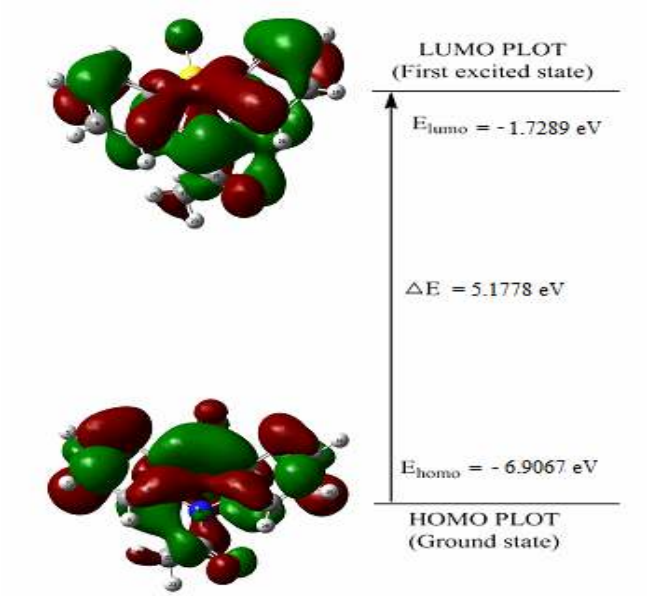

Fig. 4: HOMO-LUMO plot of APTZ molecule.

In HOMO the main electronic transition is occurred at C=C bonds of all the rings, S atom of the rings R2 and carbonyl group (in small amounts), while in LUMO the charge density is mainly accumulated at CC bond in rings.

Table 1. Electronic transitions, absorption wavelength λ_{max} (nm), excitation energy (eV), oscillator strengths (f), frontier orbital energies (eV) and dipole moment (Debye) of APTZ.

Excited States	Calculated								Transition type/ assignments
	Gas Phase				Benzene solution				
	λ_{max} (nm)	Transitions	E(ev)	Oscillator strength (f)	λ_{max} (nm)	Transitions	E(ev)	Oscillator strength (f)	
1	278	H→L	4.4594	0.0549	280	H→L	4.4249	0.0838	$\pi\rightarrow\pi^*$
2	256	H-1→L	4.8445	0.0152	251	H→L+1	4.9486	0.0983	
3	252	H→L+1	4.9107	0.0537	246	H-3→L	5.0408	0.0271	
4	244	H→L+2	5.0754	0.0283	244	H→L+2	5.0852	0.0489	$\pi\rightarrow\pi^*$
5	236	H-3→L	5.2463	0.0081	235	H-5→L	5.2858	0.0160	
6	231	H-5→L	5.3783	0.0091	225	H→L+3	5.4995	0.0215	
7	226	H-7→L	5.4730	0.0122	222	H→L+4	5.5930	0.0434	
8	221	H-1→L+2	5.154	0.0152	221	H- 6→L	5.6169	0.0224	

	E_{HOMO} (eV)	E_{LUMO} (eV)	ΔE (eV)	μ(D)
Gas	-6.9067143	-1.7289234	5.1777909	6.1429
Benzene	-6.8639946	-1.7066112	5.1573834	7.0474

HOMO = 71, LUMO = 72

The calculated frontier orbital energies, absorption wavelengths (λ_{max}), oscillator strengths (f), excitation energies (E) and dipole moments (μ) for gas phase and benzene solvent environment (integral equation formalism-polarizable continuum model, IEF-PCM) using the TD-DFT/6-31G method are illustrated in Table 1. This electronic absorption corresponds to the transition from the ground to the first excited state and is mainly described by one electron excitation from the HOMO to the LUMO. The first allowed-dipole transition in the gas phase was calculated about 278 nm with oscillator strength 0.0549. The next transitions were calculated about 252, 244 and 221 nm with oscillator strengths 0.0537, 0.0283 and 0.0152, respectively. The transitions $\pi \rightarrow \pi^*$ are the main observed transitions.

3.4. Vibrational assignment

An APTZ molecule has 30 atoms and hence gives 84 (3N-6) fundamental modes of vibration. All of them are both the Raman and IR active. Since the vibrational wavenumbers calculated by DFT methods are higher than their precise values, so they were scaled down by the wavenumber linear scaling procedure (WLS) [ν_{obs}/ν_{cal} = (1.0087 – 0.0000163 x ν_{cal}) cm^{-1}] of Yoshida *et al*. [33]. However, there are different scaling factors, but the vibrational wavenumbers calculated uniformly scaled with only one scaling factor [34,35] are often in good agreement to the observed ones.

The Raman scattering cross sections, $\partial\sigma_j/\partial\Omega$, which are proportional to the Raman intensities, may be calculated from the Raman scattering amplitude and predicted wavenumbers for each normal modes using the relationship [36,37]

$$\frac{\partial \sigma_j}{\partial \Omega} = \left(\frac{2^4 \pi^4}{45}\right) \left(\frac{\left(\nu_0 - \nu_j\right)^4}{1 - \exp\left[\frac{-hc\nu_j}{kT}\right]} \right) \left(\frac{h}{8\pi^2 c \nu_j}\right) S_j$$

where S_j and υ_j are the calculated scattering activities and the predicted wavenumbers, respectively, of the j^{th} normal mode, υ_o is the Raman excitation wavenumber and h, c and k are the universal constants.

Assignments have been made on the basis of relative intensities, energies, line shape and potential energy distribution. All the vibrational bands have been assigned satisfactorily, together with the IR and the Raman intensities. The assigned wavenumbers of the vibrational modes calculated at the HF and B3LYP level with the basis set 6-311++G(d,p) along with their PED are given in Table 2.

In the APTZ molecule, there are three rings with different functional groups as shown in Fig. 1. The vibrational assignments of these rings along with some functional groups have been discussed separately. The calculated IR and Raman spectra are given in the Figs. 5 and 6, respectively.

3.4.1. CH3 vibrations

The title molecule has one methyl group associated with different types of vibrations: like symmetric and asymmetric stretching, deformations and rocking as listed in Table 2. Asymmetric stretching of CH3 is at 3039/3017 cm^{-1} in scaled DFT having intensities of 5.43/3.53 a.u in the IR and 258.68/292.55 a.u in the Raman spectra, respectively. The symmetric stretching is calculated at 2927 cm-1 (contribution 100%). This band is weak in IR band with intensity of 2.81 a.u. and strong intensity of 824.08 a.u. in the Raman spectra. The asymmetric bending modes of this group are calculated at 1461 and 1447 cm^{-1}, while the symmetric bending mode is calculated around 1380 cm^{-1}. The rocking vibration is calculated at 1043 and 1017 cm^{-1} in the scaled DFT, which is weaker in intensity in the IR spectrum in comparison to that in the Raman spectrum.

Table 2. Calculated wavenumbers (in cm^{-1}), IR and Raman intensities (in a.u.).

Unscaled	Scaled		Intensity		PEDa (%)
DFT	HF	DFT	IR	Raman	
3232	3228	3090	0.31	382.37	R1[υ(CH)](97)
3203	3213	3063	6.21	1517.81	R3[υ(CH)](96)
3202	3212	3063	8.53	585.95	R1[υ(CH)](95)
3198	3205	3059	2.15	174.26	R3[υ(CH)](98)
3190	3197	3052	6.43	696.38	R1[υ(CH)](98)
3189	3196	3051	5.87	487.54	R3[υ(CH)](99)
3176	3182	3040	3.5	309.77	R1[υ(CH)](99)
3176	3181	3039	1.74	271.13	R3[υ(CH)](99)
3151	3152	3017	5.43	258.68	υa(CH3)(99)
3120	3123	2988	3.53	292.55	$\upsilon_a(CH_3)$(100)
3052	3061	2927	2.81	824.08	$\upsilon_s(CH_3)$(100)
1760	1906	1725	321.27	503.6	[υ(C=O)](78)+ρ[C=O](7)+[υ(CC)](5)
1636	1750	1607	18.47	370.17	R3[υ(CC)(32)+δ_{in}(CH)(6)]+R1[υ(CC)(22)+δ_a(5)]
1624	1742	1595	32.61	1411.67	R1[υ(CC)(35)+δ_{in}(CH)(11)+δ_a(6)]+R3[υ(CC)](27)
1619	1733	1591	13.48	527.92	R1[υ(CC)(35)+δ'a(5)]+R3[υ(CC)](27)+R2[υ(CC)]7)
1609	1719	1581	2.36	178.71	R1[υ(CC)](31)+R3[υ(CC)(27)+δ_{in}(CH)](8)]+R2[υ(CC)](9)
1507	1610	1483	52.39	7.75	R1[δ_{in}(CH)(25)+υ(CC)](11)]+R3[δ_{in}(CH)](24)+υ(CC)](6)+R2[υ(CC)](8)
1492	1595	1468	90.55	105.5	R1[δ_{in}(CH)(25)+υ(CC)(19)]+R3[δ_{in}(CH)](20)+R2[υ(CC)(8)+υ(CN)(8)]
1484	1578	1461	18.95	202.89	[δ_a(60)+δ'$_a$(22)+ρ'(6)](CH_3)
1481	1574	1458	13.74	21.16	R3[δ_{in}(CH)(33)+υ(CC)(21)]+R1[δ_{in}(CH)](14)+R2[δ_{trig}](7)
1476	1572	1454	5.69	26.18	R1[δ_{in}(CH)(38)+υ(CC)(22)]+R3[δ_{in}(CH)](11)+υ(CC)(8)]
1469	1559	1447	7.43	128.29	[δ'$_a$(61)+δ_a(19)+ρ(9)](CH_3)
1399	1509	1380	40.71	79.17	δ_s[CH_3](88)+[υ(CC)](7)
1340	1427	1323	12.27	376.6	R1[υ(CC)](49)+R3[υ(CC)](26)+R2[υ(CC)]6)
1332	1405	1315	62.21	319.78	R2[υ(CN)(26)+δ_{in}(NC21)(6)]+R3[υ(CC)(24)+δ_{in}(CH)(7)]
1326	1396	1309	10.69	307.35	R1[υ(CC)(36)+δ_{in}(CH)(8)]+R3[υ(CC)(25)+δ_{in}(CH)(9)]+R2[υ(CC)](9)
1309	1369	1293	61.86	190.42	R1[δ_{in}(CH)](25)+υ(NC21)(11)]+R3[δ_{in}(CH)(22)+υ(CC)(5)]+R2[δ_{trig}](13)
1272	1345	1257	277.81	400.6	R2[$\upsilon_a(SO_2)$](85)
1257	1308	1243	97.12	1261.13	R2[υ(NC21)(16)+δ_{in}(CH)(18)+υ(CC)(8)+υ(CN)(22)]
1256	1300	1241	134.26	625.29	R3[δ_{in}(CH)](26)+υ(CC)(11)]+R2[υ(CN)](17)+R1[υ(NC21)](13)
1213	1294	1200	64.05	1000.42	R2[υ(CN)(15)+υ(CC)(12)+δ_{in}(CH)(11)+υ(NC21)(7)+δ_{trig}(6)]+[υ(CC)](11)+δ[C=O](9)+[ρ[CH_3](5)
1187	1251	1174	0.46	62.57	R1[δ_{in}(CH)(55)+υ(CC)(9)]+R3[δ_{in}(CH)(19)+δ_{in}(CH)(9)]
1186	1233	1173	0.71	356.79	R3[δ_{in}(CH)(54)+υ(CC)(10)]+R1[δ_{in}(CH)](23)
1159	1213	1147	41.18	654.94	R1[δ_{in}(CH)(22)+υ(CC)(20)]+R3[δ_{in}(CH)(15)+υ(CC)(11)]+R2[υ(CS)](13)
1153	1188	1142	3.5	123.02	R3[δ_{in}(CH)(23)+υ(CC)(21)]+R1[υ(CC)(15)+δ_{in}(CH)(15)]+R2[υ(CS)](10)
1124	1185	1113	123.48	1162.02	R2[$\upsilon_s(SO_2)$(32)+υ(CS)(12)]+R1[δ_{trig}](9)+R3[δ_{trig}](9)
1083	1159	1073	26.3	29.9	R3[δ_{trig}(18)+δ_{in}(CH)(8)+υ(CC)(7)]+R1[δ_{trig}(19)+υ(CC)(6)]+R2[υ(CS)](13)
1058	1149	1049	37.24	1602.59	R1[υ(CC)](22)+δ_{in}(CH)(8)+[ρ'(13)+ρ(8)](CH3)+R2[$\upsilon_s(SO_2)$](14)+ω[C=O](5)+[R3[υ(CC)(5)+δ_{trig}(5)]
1057	1144	1048	0.46	248.47	R3[υ(CC)(37) +δ_{in}(CH)(10)+δ_{trig}(7)] +R1[υ(CC)(21)+δ_{trig}(9)]

1052	1115	1043	0.59	839.1	[ρ'(43)+ρ(7)+δ_a(5)](CH$_3$)+ω[C=O](12)+R1[υ(CC)](6)
1048	1113	1039	42.63	1154.47	R2[υ_s(SO$_2$)](31)+R3[δ_{trig}(10)+υ(CC)(8)]+R1[δ_{trig}(17)+υ(CC)(8)]
1026	1107	1017	32.89	197.49	[ρ(38)+ρ'(10)](CH$_3$)+R1[δ_{trig}(11)+υ(NC21)(7)]+ρ[C=O](5)+[υ(CC)](5)+δ'a[CH$_3$](5)
1003	1106	996	0.05	6.51	R3[oop(CH)(81)+puck(12)]
1002	1103	994	0.09	6.74	R1[oop(CH)(83)+puck(11)]
991	1078	984	2.79	197.74	R3[δ_{trig}](25)+R1[oop(CH)(12)]+R2[δ_{trig}(6)+δ_{in}(NC21)(6)]+[υ(CC)](8)+ρ[C=O](6)
974	1076	967	0.87	13.73	R3[oop(CH)(88)+τ'(5)]
970	1057	963	0.85	43.24	R1[oop)CH)(84)+τ'(5)]
907	988	902	7.46	106.16	[υ(CC)](20)+R1[δ_{trig}(15)+υ(CC)](7)+R3[oop(CH)](7)+R2[υ(CN)](6)+ρ[CH$_3$](5)
888	978	883	0.14	24.54	R3[oop(CH)(81)+puck(5)]
883	960	878	0.43	45.94	R1[oop(CH)(85)+puck(7)]
780	856	777	65.95	18.38	R3[oop(CH)(53)+puck(7)]+R1[oop(CH)](16)+R2[puck](6)
772	848	769	7.95	8.61	R1[oop(CH)](61)+R3[oop(CH)](22)
760	838	757	13.83	205.58	R3[puck(39)+oop(CH)(8)]+R1[puck](17)+R2[puck](17)
744	812	741	29.41	38.51	R1[puck(25)+oop(CH)(7)]+R3[δ_a(14)+puck(10)]+R2[υ(CS)]7)
740	808	737	2.75	49.1	R1[δ_a(16)+δ'_a(5)+puck(12)+R3[δ_a(11)+δ'_a(5)+puck(7)]+R2[υ(CS)(7)+υ(NC21)(5)]
732	795	730	41.02	52.37	R1[puck(24)+δ'_a(6)]+R3[puck](21)+R2[ω(SO$_2$)(8)+υ(CS)(10)+τ(6)]
680	734	678	0.96	1560.6	R1[δ'_a(24)+δ_a(5)]+R3[δ'_a(17)+δ_a(10)+puck(5)]+R2[υ(CS)](8)
650	696	649	6.25	59.28	R3[δ'_a](39)+R1[δ_a(15)+δ'_a(8)]+ρ[C=O](7)+[υ(CC)](6)
618	667	618	24.55	111.18	[ω(29)+δ(10)](C=O)+R2[δ_{trig}(11)+oop(NC21)(10)]+ρ[CH$_3$](6)+R1[δ_a](6)
592	646	591	26.66	239.37	[ω(13)+δ(9)](C=O)+R1[puck(12)+τ(7)]+R2[oop(NC21)(5)+puck(5)]+ρ'[CH$_3$](6)
581	638	581	45.4	58.91	R2[ω(SO$_2$)](27)+R3[puck(16)+τ(10)+δ_a(6)]+R1[δ'_a](9)
561	630	561	53.14	590.6	R2[δ(SO$_2$)(26)+δ_{trig}(8)+δ'_a(7)]+R1[τ'](5)+R3[τ](5)+τ(C11C12)(5)
555	606	555	13.39	309.64	R2[puck(16)+δ_{trig}(7)+ρ(SO$_2$)(5)]+ω[C=O](16)+R3[τ](10)+R1[τ](7)+ρ'[CH$_3$](5)
516	567	516	11.61	34.39	R1[τ](29)+R3[τ](22)+R2[τ](15)
502	553	502	7.58	81.73	R3[τ'](18)+δ[C=O](14)+R2[ρ(SO$_2$)(12)+τ'(6)]+τ(C1C10)(9)+R1[τ'(7)+δ_a(6)]+τ(C11C12)(5)
464	519	464	8.81	249	R2[δ(SO$_2$)(23)+oop(NC21)(9)+δ_{trig}(8)+τ'(7)]+R3[τ](16)+τ(C1C10)(13)+δ[C=O] (5)
458	505	458	1.63	301.3	R1[τ'](30)+R3[τ'(10)+τ(10)]+τ(C11C12)(13)+τ(C1C10)(8)+R2[γ(SO$_2$)](6)
411	442	412	10.79	887.25	ρ[C=O](28)+R3[τ'(11)+τ(6)+δ'_a(8)]+R2[υ(CN)](10)
397	436	398	8.74	409.44	R2[δ_a(36)+δ'_a(16)+υ(CS)(10)]+R1[τ'](9)
381	414	382	2.12	727.17	R1[τ'](15)+[ρ(14)+δ(6)](C=O)+R2[ρ(SO$_2$)(11)+τ'(7)+υ(CS)(5)]+R3[τ](5)
353	387	354	1.29	2098.6	R3[τ'(18)+τ(6)]+R1[τ'](15)+R2[υ(CS)(6)+υ(CN)(5)]
319	356	320	1.12	867.18	R2[δ'_a(29)+δ_a(13)+υ(NC21)(5)]+[δ(11)+ρ(5)](SO$_2$)+R3[τ'](9)
312	347	313	4.36	268.87	R2[(γ(15)+ω(5))(SO$_2$)+υ(CS)(11)+δ_{in}(NC21)(8)]+R1[τ'(11)+τ(9)]+R3[τ'](6)+ρ[C=O](6)
280	306	281	1.99	197.05	R3[τ](19)+R1[τ](11)+R2[oop(NC21)(6)+(ρ(6)+δ(5)(SO$_2$))+υ(CS)(7)+δ_{trig}(5)]+τ(C1C10)(10)+τ(C11C12)(5)

242	274	243	4.75	1023.84	R2[(ω(20)+γ(18))(SO_2)+υ(CS)(16)+δ_a(11)]+R3[δ_a](5)
205	224	206	1.75	636.7	R2[γ(SO_2)(23)+δ_{in}(NC21)(18)]+R3[τ](15)+τ(C1C10)(14)+R1[τ](6)
193	214	194	0.26	784.79	R2[oop(NC21)(13)+ρ(SO_2)(10)+υ(CS)(10)+δ_{trig}(5)+τ'(5)]+R1[τ](12)+R3[δ_a](6)
150	168	151	2.18	3124.11	τ(C11C12)(28)+τ(C1C10)(25)+R2[γ(SO_2)(14)+δ_{in}(NC21)(8)]+R3[τ'](5)
128	147	129	0.12	6552.24	τ(C21C22)(26)+R2[puck(25)+ρ(SO_2)(5)]+τ(C11C12)(10)+τ(C1C10)(8)+ρ'[CH_3](6)+R3[τ](6)
115	131	116	0.2	5116.14	τ(C21C22)(29)+τ(C11C12)(22)+R2[puck(11)+R2τ'(7)]+ρ'[CH_3](8)
97	114	98	0.94	1060.01	R2[τ](26)+R2[τ'(12)+δ_{in}(NC21)(7)]+τ(C11C12)(18)+τ(C21C22)(10)+τ(C1C10)(7)
75	81	76	0.59	19405.86	R2[oop(NC21)(45)+τ'(5)]+τ(C1C10)(16)+τ(C21C22)(10)+τ(C11C12)(6)
71	76	71	4.07	1737.43	τ(C21C26)(63)+R2[δ_{in}(NC21)](5)+τ(C1C10)(5)
51	50	52	4.64	23135.09	R2[τ'](24)+oop(NC21)(14)+τ(5)]+τ(C21C26)(18)+τ(C21C22)(14)

Proposed assignments and potential energy distribution (PED) for vibrational normal modes.
Types of vibration: ν, stretching; δ, deformation (bending), scissoring; oop, out-of-plane bending; ω, wagging; γ, twisting; ρ, rocking; τ, torsion.
[a]Potential energy distribution (contribution ≥ 5).

3.4.2. C= O vibrations

A carbonyl (C=O) group is connected at the nitrogen atom of ring R2. Regarding to this group; stretching, bending, rocking and wagging modes of vibrations are observed. The stretching of C=O is calculated at 1725 cm^{-1} (contribution 78%). The deformation and wagging calculated at 618 and 591 cm^{-1} are the mixed modes. The rocking vibration is calculated at 412 cm^{-1} (contribution 28%) with the intensities of 10.79 a.u. in the IR spectrum and 887.25 a.u. in the Raman spectrum, respectively.

3.4.3. Ring R1 vibrations

Ring R1 has four CH moieties; hence one can expect four stretching modes associated to this group. All these modes are pure in the range 3090-3040 cm^{-1} and have very weak in intensity in the IR spectrum. The mixed in-plane deformations are calculated at 183, 1468, 1454, 1293, 1174 and 1147 cm^{-1}. The out-of-plane bending modes are calculated at 994, 963, 878 and 769 cm^{-1}.

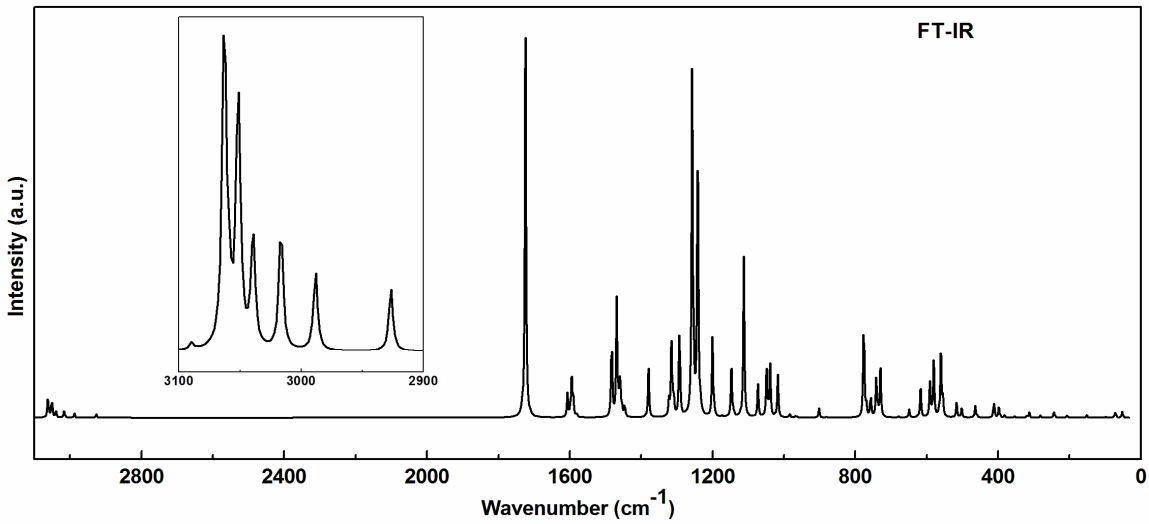

Fig. 5. Theoretical IR spectra between the ranges 0-3100 cm^{-1}.

The C-C stretching is stronger in intensity in the Raman spectrum than in the IR spectrum.
These modes are calculated below 1595 cm^{-1}. Around 741/730 cm^{-1} and 737/678 cm^{-1} are the puckering and deformation of the ring, respectively. The ring torsion is calculated at 516, 458 and 382 cm^{-1} in the mixed modes.

3.4.4. Ring R2 vibrations

Two important functional groups SO_2 and $–COCH_3$ are connected with this ring R2. The six fundamental modes of vibrations are assigned with SO_2 group; namely symmetric, asymmetric stretch, deformation and rocking, which belong to polarized in-plane vibrations. In addition to that, SO_2 wagging and twisting modes would be expected to be depolarized out-of-plane symmetry species. The SO_2 asymmetric stretching having contribution of 85% in PED is calculated at 1257 cm^{-1}. The symmetric stretching is calculated at 1113/1029 cm^{-1}, which have strong Raman intensities of 1162.02/1154.47 units. The deformations are calculated at 561 and 464 cm^{-1}. The wagging and twisting vibrations are calculated at 581/243 cm^{-1} and 313/206 cm^{-1}, respectively. Highly mixed rocking mode with low contribution in PED is calculated below 555 cm^{-1}.
CN stretching is calculated at 1315 and 1200 cm^{-1}. NC21 stretching is calculated at 1243 cm^{-1}, which has weak IR and strong Raman intensities as listed in Table 2.

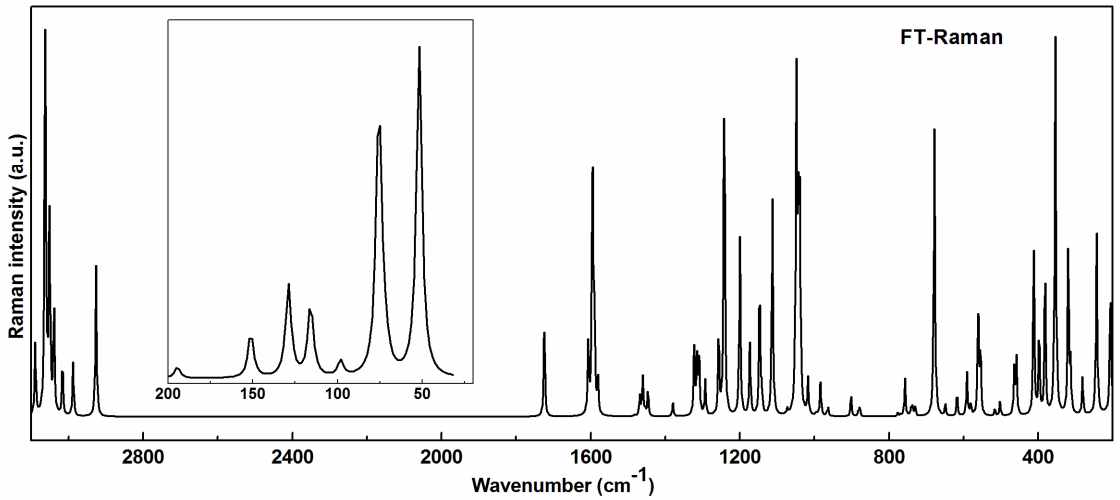

Fig. 6. Theoretical Raman spectra between the ranges 20-3200 cm-1.

3.4.5. Ring R3 vibrations

Ring R3 has also four CH moieties; hence four CH stretching modes are assigned between the range 3063-3039 cm^{-1}. The CC stretching of the ring is calculated at 1607/1048 cm^{-1}. The trigonal ring deformation is calculated at 1073 cm^{-1} with weak intensities both in the IR and the Raman spectra. The ring puckering, asymmetric deformation and the ring torsion are calculated at 757, 649 and 502 cm^{-1}, respectively.

4. Conclusion

The equilibrium geometries and harmonic vibrational wavenumbers of all the 84 normal modes of the APTZ molecule were determined and analyzed both at DFT (B3LYP) and HF levels of theory employing the 6-311++G(d,p) basis set. These theoretical vibrational assignments along with the electronic transitions are important to understand the molecular structure and biological activity of the title

molecule. The IR and the Raman spectra were presented, and the vibrational bands were assigned on the basis of the PED obtained from the DFT calculations. Information about the size, shape, charge density distribution and structure-activity relationship of the APTZ molecule has been obtained by mapping electron density isosurface with ESP and MESP. HOMO - LUMO made very clearly the involvement of charge transfer between the donor and acceptor groups.

Acknowledgements

The authors are grateful to the University Grants Commission, Nepal, and Alexander von Humboldt Foundation, Germany, for providing partial financial assistance.

References

[1] S.A. Alkalis, G. Beck and M. Grätzel, J. Am. Chem. Soc., 97 (1975) 5723.
[2] Y. Dixit, R. Dixit, N. Gautam and D.C. Gautam, E-J. Chem., 5(S1) (2008) 1063.
[3] C. Chan, H. Yin, J. Garforth, J.H. McKie, R. Jaouhari, P. Speers, K.T. Douglas, P.J. Rock, V. Yardley, S.L. Croft, and A.H. Fairlamb, J. Med. Chem., 41 (1998) 148.
[4] B.R. Henry and M. Kasha, J. Chem. Phys., 47 (1967) 3319.
[5] M.A. Wuonola, M.G. Palfreyman, N. Motohashi, M. Kawase, S. Gabay, R.R. Gupta and J. Molnar, Anticancer Res., 18 (1998) 337.
[6] J. Molnar, A. Hever, I. Fakla, J. Fischer, I. Ocsovaki, and A. Aszalos, Anticancer Res., 17 (1997) 481.
[7] M.A. Wuonola, M.G. Palfreyman, N. Motohashi, M. Kawase, S. Gabay and J. Molnar, J. Anticancer Res., 17 (1997) 3425.
[8] M.A. Wuonola, M.G. Palfreyman, N. Motohashi, M. Kawase, S. Gabay, J. Nacsa, and J. Molnar, J. Anticancer Res., 17 (1997) 3409.
[9] I.K. Pajeva and M. Wiese, Quant. Struct-Act. Relat. ,16 (1997) 1.
[10] I.K. Pajeva, M. Wiese, H.P. Cordes, and J.K. Seydel, J. Cancer Res. Clin. Oncol., 122 (1996) 27.
[11] R.A. Singh, R. Singh, O.S. Rao, and S.M. Verma, Mol. Cryst. Liq. Cryst., 237 (1993) 419.
[12] M. Pampallona, A. Ricci, B. Scrosati and C.A. Vincent, J Appl Electrochem., 6 (1976) 269.
[13] R. Singh and R.A. Singh, Mol. Cryst. Liq. Crys.t Sci. Technol. Sect., 8C (1997) 187.
[14] M. Alconea Palafox, M. Gil, J.L. Núñez and G. Tardajos, Int. J. Quant. Chem., 89 (2002) 147.
[15] R. Sharma, P. Samadhiya, S.D. Srivastava and S.K. Srivastava, J. Serb. Chem. Soc., 77(1) (2012) 17.
[16] B.D. Joshi, A. Srivastava, P. Tandon and S. Jain, Spectrochim. Acta. A, 82 (2011) 270.
[17] Q. Wang, L. Yang, Z. Xu and Y. Sun, Acta Cryst. E ,65 (2009) 1978.
[18] P. Hohenberg and W. Kohn, Phys. Rev. B, 136B (1964) 864.
[19] M.J. Frisch, G.W. Trucks, H.B. Schlegel. G.E. Scuseria, J.R. Cheeseman, M.A. Robb, G. Scalmani, V. Barone, B. Mennucci, G.A. Petersson, H. Nakatsuji, M. Caricato, X. Li, H.P. Hratchian, A.F. Izmzylov, J. Bloino, G. Zheng, J.L. Sonnenberg, M. Hada, M. Ehara, K. Toyota, R. Fukuda, J. Ishida, M. Hasegawa, T. Nakajima, Y. Honda, O. Kitao, H. Nakai, T. Vreven, J.A. Montgomery, Jr., J.E. Peralta, F. Ogliaro, M. Bearpark, J.J. Heyd, E. Brothers, K.N. Kudin, V.N. Staroverov, R. Kobayashi, J. Normand, A. Raghavachari, A. Rendell, J.C. Burant, S.S. Iyengar, J. Tomasi, M. Cossi, N. Rega, J.M. M illan, M. Klene, J.E. Knox, J.B. Cross, V. Bakken, C. Adamo, J. Jaramillo, R. Gomperts, R.E. Stratmann, O. Yazyev, A.J. Austin, R. Cammi, C. Pomelli, J.W. Ochterski, R.L. Martin, K. Morokuma, V.G. Zakrzewski, G.A. Voth, P. Salvador, J.J. Dannerberg, S. Dapprich, A.D. Daniels, J. Farkas, B. Foresman, J.V. Ortiz, J. Cioslowski, and D.J. Fox, GAUSSIAN 09, Revision, Gaussian, Inc., Wallingford CT, 2009.
[20] C.T. Lee, W.T. Yang and R.G. Parr, Phys. Rev. B, 37 (1988) 785.
[21] A.D. Becke, J. Chem. Phys., 98 (1993) 5648.
[22] G.A. Petersson and M.A. Allaham, J. Chem. Phys., 94 (1991) 6081.
[23] G.A. Petersson, A. Bennett, T.G. Tensfeldt, M.A. Allaham and W.A. Shirley, J. Mantzaris, J. Chem. Phys., 89 (1988) 2193.
[24] P. Pulay, G. Fogarasi, F. Pang and J.E. Boggs, J. Am. Chem. Soc., 101 (1979) 2550.
[25] G. Fogarasi, X. Zhou, P.W. Taylor and P. Pulay, J. Am. Chem. Soc., 114 (1992) 8191.

[26] J.M.L. Martin and C.V. Alsenoy, Gar2ped, University of Antwerp (1995).
[27] G.A. Zhurko and D.A. Zhurko, Chemcraft (2005).
[28] P. Politzer and D. G. Truhlar, Chemical Applications of Atomic and Molecular Electrostatic Potentials, Plenum, New York (1981).
[29] S. R. Gadre, P. K. Bhadane, S. S. Pundlik and S. S. Pingale, Molecular Electrostatic Potentials Concepts and Applications, ed. J. S. Murray and K. D. Sen (1996) pp. 219.
[30] P. Politzer, M. E. Grice, J. S. Murray and J. M. Seminario, Can. J. Chem., 71 (1993) 1123.
[31] C. H. Suresh, P. Alexander, K. P. Vijayalakshmi, P. K. Sajith and S. R. Gadre, Phys. Chem. Chem. Phys., 10 (2008) 6492.
[32] R.M. Issa, M.K. Awad and F.M. Atlam, Appl. Surf. Sci., 255 (2008) 2433.
[33] H. Yoshida, K. Takeda, J. Okamura, A. Ehara, and H. Matsurra, J. Phys. Chem. A, 106 (2002) 3580.
[34] M.W. Wong, Chem. Phys. Lett., 256 (1996) 391.
[35] A.P. Scott and L. Radom, J. Phys. Chem., 100 (1996) 16502.
[36] G.A. Guirgis, P. Klaboe, S. Shen, D.L. Powell, A. Gruodis, V. Aleksa, C.J. Nielsen, J. Tao, C. Zheng and J.R. Durig, J. Raman Spectrosc., 34 (2003) 322.
[37] P.L. Polavarapu, J. Phys. Chem., 94 (1990) 8106.